Analysis of Magnet Axial Temperature Variation Effect on the Performance of Five-Phase Permanent Magnet assisted Synchronous Reluctance Motor

Md Khurshedul Islam, Seungdeog Choi
Department of Electrical and Computer Engineering
Mississippi State University, Starkville, MS, USA
Mi264@msstate.edu, seungdeog@ece.msstate.edu

***Abstract*— This paper presents the impact of magnet axial temperature variation on the electromagnetic performance of a five-phase permanent magnet assisted synchronous reluctance motor (PMaSynRM). The torque performance, manet demagnetization, vibration and control of permanent magnet (PM) machine are highly dependent on the variation of PM temperature. Commonly, in machine control, an average radial magnet temperature is estimated and used, while the temperature variation along the axial direction is assumed as uniform. However, in practice, the magnet axial temperature variation is not uniform, and it can lead to unbalance magnetization, localized magnet hot-spot, increase in torque ripple, and machine noise. These effects can be even more crucial in the high-speed and high-power density machine. In this study, the nonuniform PM axial temperature distribution has been estimated by using a novel axial thermal model adopting the finite volume method (FVM). Furthermore, its effects on the machine performance, especially back EMF, radial force, and torque ripple, have been investigated using the 3-D FEA model. The estimated and simulated results have been validated by an innovative wireless experimental setup.**

Keywords*— *Magnet Axial Temperature, Lumped Parameter Thermal Model, Thermal analysis, PMSM,

I. INTRODUCTION

In recent years, the use of permanent magnet synchronous motor (PMSM) is overgrowing, especially in the application of electric vehicle (EVs) and hybrid electric vehicles (HEVs) because of its tremendous development in the power and torque density [1-2]. The increase in power or torque to weight ratio of PMSM has been possible by designing innovative rotor structure and placing a higher volume of rear earth magnet in the rotor. The mostly used rear earth magnets in the traction applications are neodymium-iron-boron (NdFeB) and samarium cobalt (SmCo) [3]. However, with the increase of power density, these magnets become more temperature-sensitive due to the reduction in machine size and complex geometry. An increase in the magnet temperature decreases its strength, which impacts the machine performance adversely, including torque production capability and unbalanced magnetization [4-5]. Furthermore, if the magnet temperature becomes excessive, it can cause local or global permanent demagnetization in the magnet [6]. To avoid this unwanted phenomenon, a real-time PM temperature estimation or measurement is essential to control the PMSM optimally and also to ensure healthy permanent magnet (PM) during loading conditions.

However, the measurement of PM temperature is not easy because it is not possible to mount a contact type temperature sensor on the rotor. The only possible option is to use a non-contact infrared temperature sensor, which is relatively costly and also limited to use only for surface mounted PMSM [4-5]. On the other hand, the estimation of PM temperature is possible. In literature, various methods have been reported to estimate the PM temperature during the load operation. The back EMF-based process has been reported in [7-8], where an estimated magnet flux linkage is used to estimate the magnet temperature. A differential axial temperature variation and its determination based on back-EMF harmonics have been published in [9]. This BEMF based method is limited only when the machine rotates in medium-high speed, whereas it does not work in the standstill or low speed. In [10-11], the external signal injection-based PM temperature estimation method has been reported. In this process, a high-frequency test signal is injected in the machine, and the magnet temperature is estimated from the stator reflected magnet high-frequency resistance. This external signal interfaces with the machine fundamental control signal and results in an unwanted harmonic in the command signal, which is a drawback of the external signal injection-based method. The thermal model-based method has been studied in [12-13], where an equivalent thermal circuit is modeled based on lumped parameters of a 2D model of the machine.

Any of these methods do not provide information regarding magnet axial temperature variation; they only provide an estimated average temperature considering a uniform magnet temperature variation along the axial length. However, in practice, the magnet axial temperature variation is not uniform due to complex machine geometry, uneven heat transfer system, different thermal coefficient of different material and cooling system [14-15]. Hence, ignoring this phenomenon may result in localized heat stress leading to uneven magnetization. Therefore, it is required to do a details investigation of the axial temperature variation of the electrical machine. There are some research works in the literature which reported the presence of axial temperature variation in the rotor and stator. In [16], the axial temperature variation of winding has been reported and suggested a thermal model to estimate this variation. In [17-20], the temperature variation of thermally shorted coil and magnet along the axial direction have been observed by using finite element analysis (FEA). The similar observation has been reported in [21] for high-speed PMSM by considering assembly gap and temperature Gradient. A large magnet axial temperature gradient of a high-speed PMSM supported by active magnetic bearing has been presented in [22] However,

to the best of the author's knowledge, the estimation of PM axial temperature variation and its impact on the machine performance has not been addressed in any previous work.

In this paper, the PM temperature variation along the axial direction has been estimated by using a novel 3-D axial Lumped parameter thermal model (ALPTM). The ALPTM has been modelled by modifying the conventional 2-D radial Lumped parameter thermal model (RLPTM) and augmenting it with FVM. Furthermore, the effect of magnet axial temperature variation on the machine's electromagnetic performance has been analyzed in details. Finally, the experimental validation has been done by using an innovative testing setup in the rotor of a 5-phase permanent magnet assisted synchronous reluctance motor (PMaSynRM).

II. PM Axial Temperature Estimation by ALPTM

Lumped parameter based thermal analysis has been widely used to estimate the real-time temperature of the electrical machine due to its less implementation complexity, less cost, and less computation time. Also, it is possible to use during the loading condition, and it can be modeled for almost all types of machine. Fig. 1 shows the FEA models and designed prototype (stator and rotor) of a 5-phase PMaSynRM [23], which is used in this study to develop the ALPTM model. The machine specifications are given in Table I.

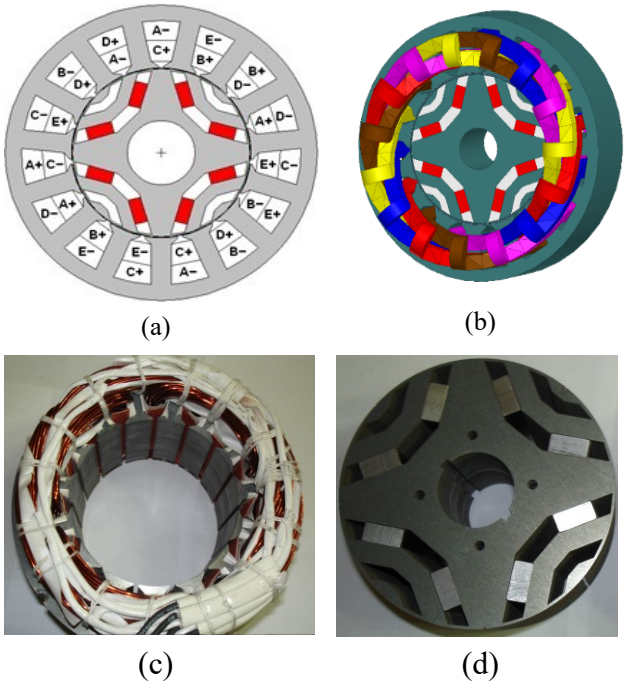

Fig. 1: FEA Model (a) 2-D, (b) 3-D; Designed prototype (c) stator, and (d) rotor.

TABLE I: PMaSynRM SPECIFICATIONS

Parameter	Value	Design Parameter	Value
Rate speed	1800 rpm	Stack length (mm)	65 mm
Rated power	3 kW	Slot/ Pole	25/4
Rated current	15.17 A	Rotor outer radius	95 mm
Rated Voltage	67 V	Air gap length	0.7 mm
Rated Torque	15.45	Magnet Material	NdFeB
Phase Number	5	Core Material	50PN470

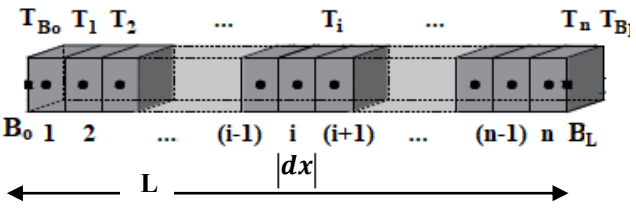

Fig. 2: Magnet segmented into n discretized nodes along axial direction.

The lamination structure of the core prevents the heat flow along the axial direction because it has a very low thermal conductivity of air ($\approx$ 0.0243Wm−1K−1) in between two consecutive laminations. In the conventional RLPTM, like the stator and rotor core, the axial heat flow of conductor coil side, magnets, and shaft are modeled as a single lumped thermal resistance under the assumption of negligible heat flow in the axial direction. However, the conductors, shaft and magnets of the motor are thermally shorted in the axial direction, which allows the flow of heat along the axial direction. Hence, with this assumption, the possibility of hot spot formation and uneven magnetization along the magnet axial length are ignored in RLPTM. However, in ALPTM, the heat flow of stator and rotor core is considered as a single lumped thermal resistance while the heat flow of coil sides, magnets, and shaft along the axial direction is estimated by using FVM. In this paper, only magnet axial temperature has been discussed in detail, while discussion on the other parts of the machine is beyond the scope of this paper.

The magnet is considered as a uniform body of cross-section area A and length L and the axial temperature variation is $T(x)$ where $0 < x < L$. In FVM, the axial two-dimensional heat flow of magnet can be represented by a second order differential equation as (1).

$$\frac{d^2T}{dx^2} + \frac{1}{\lambda A}\left[\sum_a \frac{T_a(x)-T(x)}{R'_a} + \sum_b \frac{T_b(x)-T(x)}{R'_b}\right] + \frac{\dot{q}}{\lambda} = 0 \quad \textbf{(1)}$$

The boundary nodes B_o and B_L can be defined form fig. 2, at $x = 0$ and $x = L$. The interior nodal equations ($0 \le i \le (n-1)$) can be defined as (2).

$$\frac{T_{i+1}-2T_i+T_{i-1}}{\Delta x^2} + \frac{1}{\lambda A}\left[\sum_a \frac{T_{a,i}-T_i}{R'_a} + \sum_b \frac{T_{b,i}-T_i}{R'_b}\right] + \frac{\dot{q}}{\lambda} = 0 \quad \textbf{(2)}$$

Node 1 and n are defined by (3).

$$\frac{T_{i+1}-3T_i+2T_{i-1}}{\Delta x^2} + \frac{1}{\lambda A}\left[\sum_a \frac{T_{a,i}-T_i}{R'_a} + \sum_b \frac{T_{b,i}-T_i}{R'_b}\right] + \frac{\dot{q}}{\lambda} = 0 \textbf{(3)}$$

The nodal equation for a constant boundary temperature T can be defined as (4):

$$T_{Bo} = T \text{ and } T_{BL} = T \quad \textbf{(4)}$$

The nodal equation for an isolated boundary node is as follows (5):

$$T_{Bo} - T_1 = 0 \text{ or } T_{BL} - T_n = 0 \quad \textbf{(5)}$$

Considering each element (coil, magnets, and shaft), a set of equations similar to (2)-(4) will form a tridiagonal matrix. Then, the tridiagonal matrix algorithm (TDMA) is used with

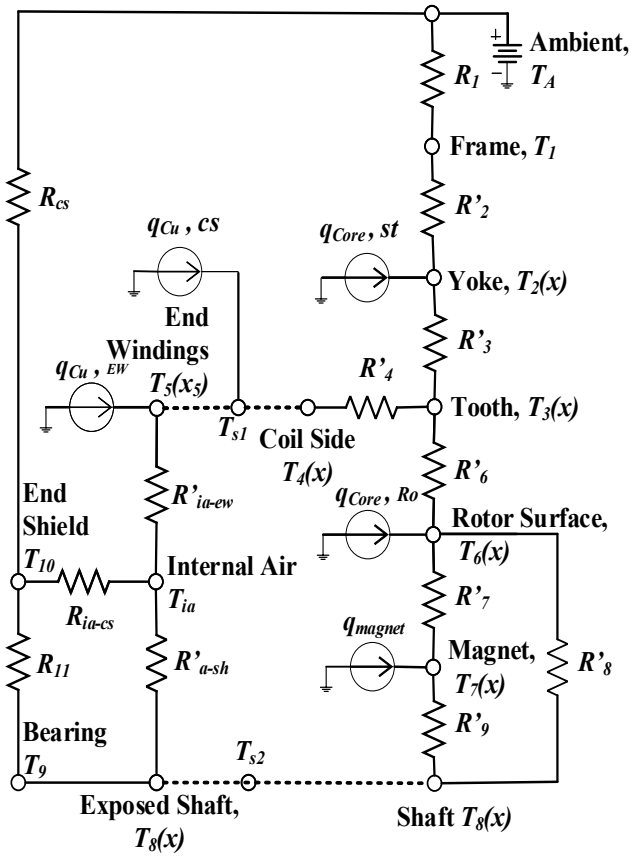

Fig. 3: An overview of ALPTM.

the help of Gauss-Seidel iteration method to derive the solution of the axial temperature distribution of each node. Fig. 3, shows an overview of the novel A-LPTM, which is used in this paper. The model is a quasi 3D model and the nodes considered as functions of the position along the axial length *(x)* along which they span as shown in the figure.

In this model, current sources represent the heat sources generated by the corresponding loss, and these are the input of the thermal model. Copper loss, core loss, and magnet loss have mainly been considered in this formulation. FEA software is used to calculate these losses. Fig. 1(a) and (b) present the 2-D and 3-D model of the machine, used in the FEA software. Copper loss is calculated based on the input RMS current and phase resistance. Core loss and magnet eddy current loss are directly calculated from FEA.

A specific loading condition (RMS phase current and rotational speed) and losses corresponding to that loading condition are applied as input to the LPTM which is developed in MATLAB script. Fig. 3(a) and (b) show the estimated temperature by both R-LPTM and A-LPTM at 5 A 1125 RPM and 15A 1800 RPM, respectively.

Firstly, as we can see, comparing with R-LPTM, A-LPTM clearly provides the added resolution of temperature variation in the axial direction. In addition, the A-LPTM data does not invalidate the credibility of the R-LPTM data at any loading condition.

Secondly, it is observed that the magnet temperature in ALPTM is not linear, unlike R-LPTM, rather it increases gradually from the edge to the center of the magnet and follows an axial axis symmetry. Though a similar phenomenon is observed in both cases, it is evident that the axial temperature variation tends to increase (e.g., with a fashion of parabolic distribution) as the speed and electric loading increase. At 5 A, 1125 RPM condition, the magnet axial temperature variation between the lowest and highest point is 0.65^oC, which further increases at 2.75^oC when loading condition is 15A, 1800 RPM.

Thirdly, the R-LPTM result is slightly higher than the result of A-LPTM; this is because the effect of axial length is ignored, and the internal air node is not considered in the R-LPTM. However, it can be seen that the difference between the R-LPTM and A-LPTM reduces as the loading condition increases from 5A to 15A.

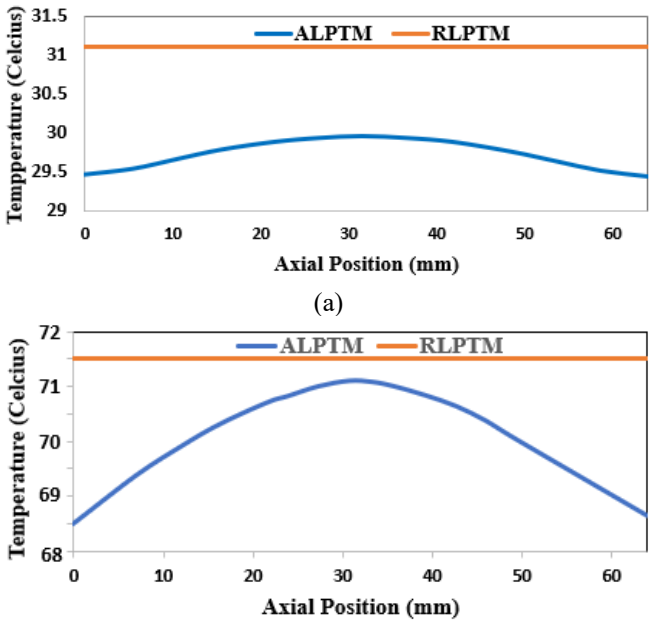

Fig. 4: Magnet axial temperature distribution by A-LPTM and RLPTM at (a) 5 A 1125 RPM and (b) 15 A 1800 RPM loading condition.

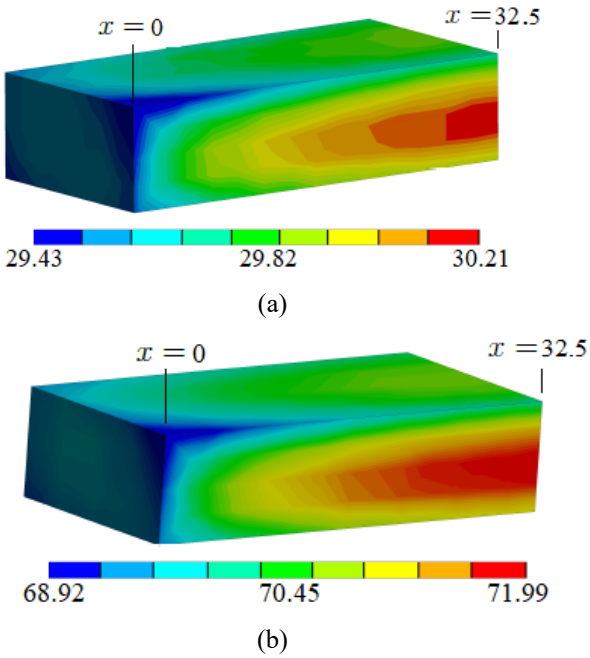

Fig. 5: Magnet axial temperature distribution by FEA with axis of symmetry at (a) 5 A 1125 RPM and (b) 15 A 1800 RPM loading condition.

TABLE II: MAGNET TEMPERATURE AT DIFFERENT LOADING CONDITION

Load Condition	5A 1125 RPM	6A 1400 RPM	8A 1500 RPM	15A 1800 RPM
Min Temp. (°C)	29.50	40.05	51.10	68.50
Max Temp. (°C)	30.15	41.10	52.70	71.35
Avg. Temp. (°C)	29.83	40.58	51.90	69.93

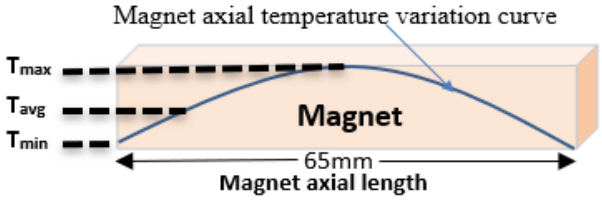

Fig. 6: Magnet temperature distribution along axial direction.

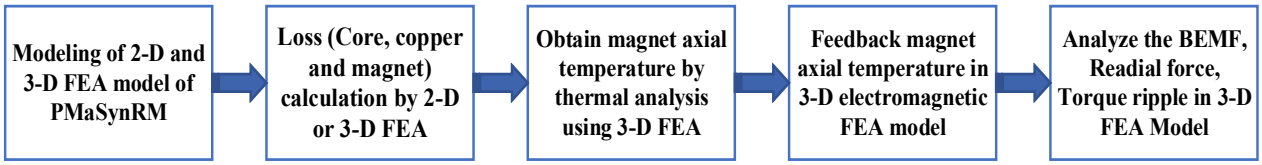

Fig. 7: Algorithm for magnet axial temperature variation effect analysis.

FEA thermal analysis is very widely used to determine accurate thermal distribution. To validate the result of A-LPTM, a 3-D steady state thermal analysis has been done in ANSYS workbench. Fig. 4(a) and (b) present the magnet axial temperature distribution obtained by 3-D thermal steady state analysis for the same loading conditions. Comparing both results, A-LPTM shows a good matching with the FEA result. It is, therefore, concluded that the magnet temperature in the axial direction is nonuniform (normal curve) instead of uniform.

III. Analysis of Magnet Axial Temperature Variation Effect

To investigate the effect of the magnet axial temperature variation on the electromagnetic performance of the machine, four different loading conditions have been considered as shown in table II. Fig.4 indicates the minimum, maximum, and average (radial temperature) temperature point of a magnet axial temperature distribution curve. The process algorithm to analyze the effect of axial temperature variation on a machine performance is shown in fig. 7.

At first, both the 2-D and 3-D FEA model of the 5-phase PMaSynRM have been designed. A five-phase winding configuration and machine design parameters are shown in fig. 1 and Table 1 respectively.

Then the electrical losses are calculated by electromagnetic analysis for the specified loading condition shown in Table II. Per-phase dc resistance is needed in FEA to calculate the copper loss, which is measured from the machine prototype. Also, for core loss calculation in FEA, loss coefficient (eddy, hysteresis, and excess) are obtained by providing different frequency vs loss curve of the core material (S_50PN470).

In the next step, these loss data are used as input to the FEA thermal model and obtain the magnet axial temperature distribution. In this case, a two-way coupling between electromagnetic and steady-state thermal has been used in ANSYS workbench. Table II shows the magnet axial temperature distribution result obtained by FEA thermal analysis. The FEA result shows a very close match with the estimated temperature obtained by ALPTM.

Then, these magnet axial temperature data are fed back to the corresponding magnet of the 3-D electromagnetic analysis model. In this case, non-uniform magnet axial temperature data is provided instead of an average uniform value. Instead of using FEA coupling between steady-state thermal and electromagnetic, these magnet temperature data are applied manually because such kind of FEA coupling does not use non-uniform temperature data; rather, it uses an average temperature. For this purpose, each magnet has been divided into 26 equal small segments of 2.5mm length along the axial direction. The number of segments is determined by an iterative process to fit the non-uniform curve perfectly in the magnet.

In the final step, the electromagnetic performance analysis has been done by using 3-D FEA model. The back-EMF, radial force, and torque ripple analysis are considered in this case.

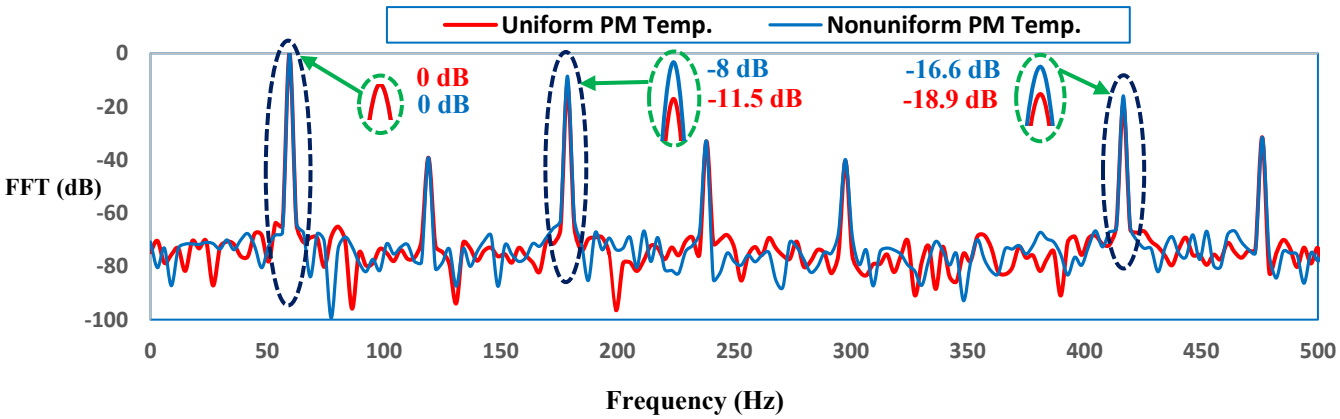

Fig 8: Back EMF spectrum at full load operation (interested frequencies are 1st ,3rd ,7th (zoomed) by dot circle).

A. *Back Electromagnetic Force (BEMF) Analysis:*

Fig. 8, shows the BEMF spectrum for both uniform and nonuniform magnet axial temperature at full load operation (15.17 A 1800 RPM). For better observation, the results are normalized with respect to fundamental harmonic of BEMF, and a logarithmic scale is used in the y-axis. The result shows that all harmonic spectrums are almost the same for the uniform and nonuniform PM temperature except the 3rd (at 180 Hz) and 7th (at 420 Hz) order harmonics. The 3rd and 7th order harmonics are increased by 3.5 dB and 2.3 dB, respectively, due to the uneven axial magnetization.

Fig.9, shows the magnetic flux density (B) at full load condition. The maximum flux density is 2.61 T occurs in the rotor bridge and the stator teeth, which is below the saturation point of the core material. Hence, there is no short circuit of magnets by the bridge, which is a possible source of BEMF harmonics. It is, therefore, confirmed that the change in harmonic contents is due to the PM uneven magnetization only, which is caused by the magnet nonuniform axial temperature variation.

Fig. 10 and 11, show the magnitude variation of fundamental and 3rd harmonics (for both uniform and non-uniform conditions) with respect to different loading PM temperatures. It is observed that the value of the relative 3rd harmonic component is increasing when the maximum value of the magnet axial temperature is increased, and 7th harmonic follows the same pattern. Therefore, it can be concluded that the fundamental harmonic of BEMF does not affect by the magnet axial temperature variation, whereas the value of dominant harmonics (3rd and 7th order for this specific machine) is increased considerably with the increase of magnet axial temperature variation.

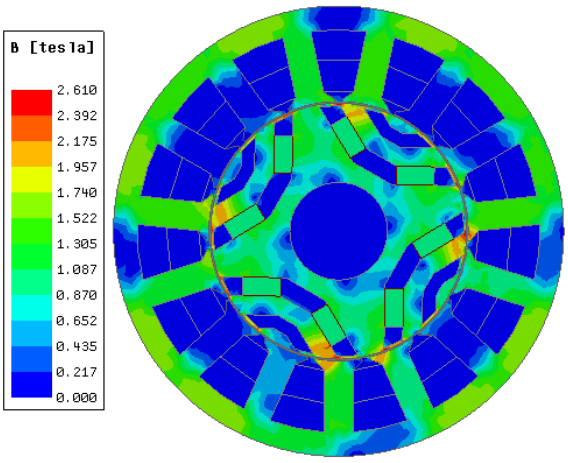

Fig. 9: Flux density distribution at 15.17 A, 1800 RPM.

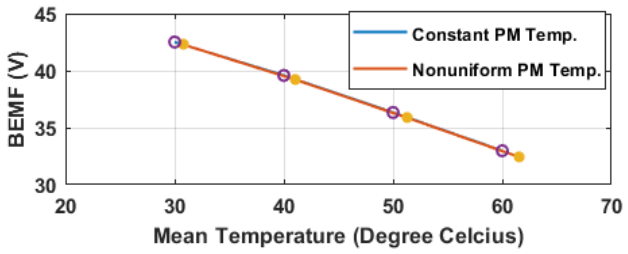

Fig. 10: Fundamental component of BEMF vs mean magnet temperature.

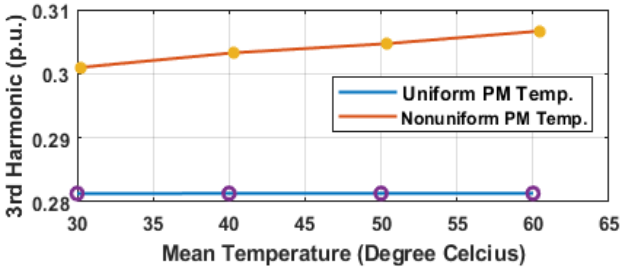

Figure 11: 3rd Harmonic component of BEMF vs mean magnet temperature.

B. *Radial Force Analysis:*

Fig. 12, shows the generated radial force (RF) on the rotor for both uniform and nonuniform magnet axial temperature at full load condition. It can be observed that the average radial force on the rotor has been increased from 173.45 N to 178.05 N due to nonuniform magnet axial temperature variation. This phenomenon will lead the magnet to create an unbalanced magnetic pull (UMP). Furthermore, UMP can cause unwanted noise and vibration in the machine, which can be estimated from the harmonic analysis of RF.

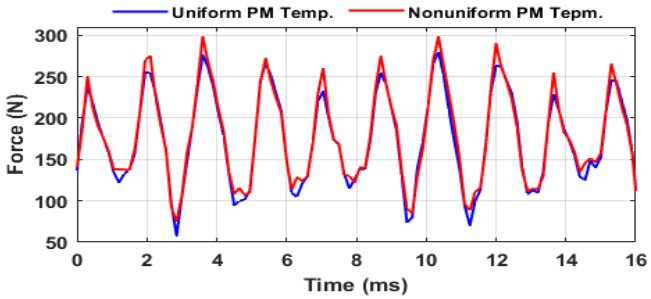

Fig. 12: Radial force comparison at full load operation.

C) *Torque Analysis:*

The magnet axial temperature variation can affect the torque ripple significantly because as mentioned earlier, the magnet axial temperature variation results in an increase of the BEMF's dominant harmonic components. Fig. 13 shows the full load electromagnetic torque at both uniform and nonuniform magnet axial temperature. It is observed that due to the magnet axial temperature variation, the average torque is reduced from 14.02 Nm to 13.96 Nm, which can be neglected but the torque ripple increases from 6.73% to 7.81%. The torque ripple is calculated by dividing the difference of maximum and minimum torque by the average torque. This torque ripple increment can lead to unwanted machine noise and vibration.

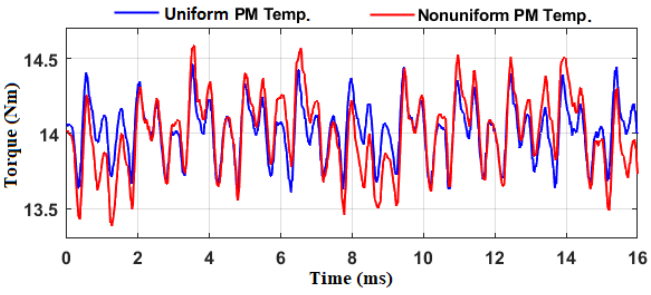

Fig. 13: Electromagnetic torque at full load operation.

TABLE III: SUMMARY OF ELECTROMAGNETIC PERFORMANCE ANALYSIS

Operating Condition	5 A -1125 RPM	6 A – 1400 RPM	8 A - 1500 RPM	15 A - 1800 RPM
THD in BEMF at uniform temp. (%)	29.32	29.38	29.41	29.45
THD in BEMF at nonuniform temp. (%)	30.18	30.492	30.71	30.78
THD increase in BEMF	2.85%	3.65%	4.23%	5.01%
Average Torque at uniform temp. (Nm)	15.320	14.968	14.508	14.028
Average Torque at nonuniform temp. (Nm)	15.310	14.908	14.440	13.96
Average Torque decrease	<<1%	<<1%	<<1%	<<1%
Torque ripple at uniform temp. (%)	5.864	5.476	6.149	6.737
Torque ripple at nonuniform temp. (%)	6.183	5.957	6.935	7.781
Torque Ripple Increase	5.177%	8.069%	11.335%	13.42%
Radial Force on rotor at uniform temp. (N)	133.117	150.413	165.411	173.448
Radial Force on rotor at nonuniform temp. (N)	133.9765	152.4050	168.6026	178.0461
Radial force on motor increase	1%	2.3%	3.2%	4.6%

A summary of complete electromagnetic performance analysis under both uniform and nonuniform magnet axial temperature is given in the table III.

IV. Experimental Validation

Experimental analysis has been performed to validate the magnet axial temperature variation and performance analysis. Fig. 14, shows an overview of the complete experimental setup of 5-phase PMaSynRM with a 3-kW DC generator (load). The current density of the motor is 4.5 A/mm^2; hence a normal air cooling is used. In order to measure the magnet real-time temperature variation data and collect it without interfering with the motor operation, an innovative wireless data acquisition and transmission setup are designed, as shown in fig. 15. Five PT100RTD sensors have been attached on the magnet to observe the magnet axial temperature distribution. The sensors have a temperature range of -73^oC to 260^oC with a tolerance value of $\pm 0.06\%$. Fig. 13, shows the position of the sensors along with the magnet axial length. The wireless PCB has been mounted on the rotor, which contains an A/D converter and a Bluetooth transducer.

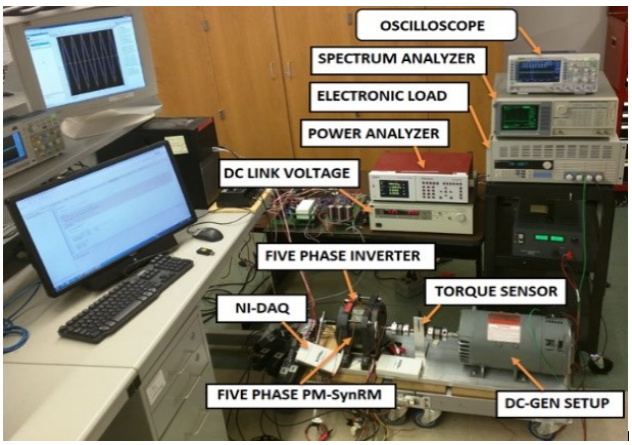

Fig. 14: Experimental Setup overview.

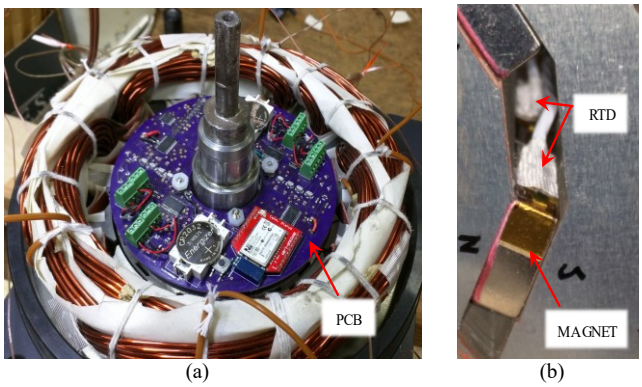

(a) (b)

Fig. 15: (a) PCB for wireless data transmission, (b) sensor on magnet

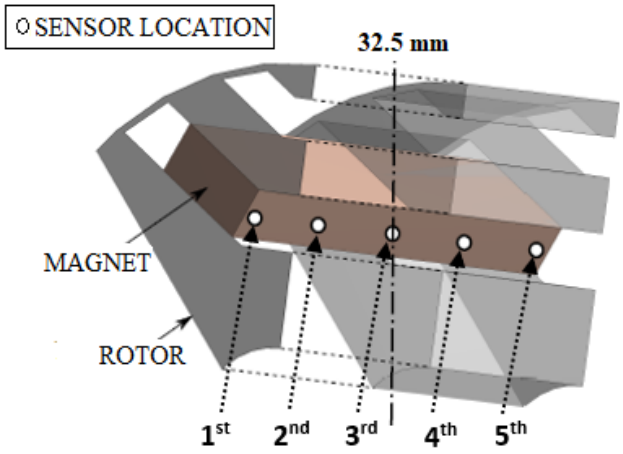

Fig. 16: Sensor location on magnet along axial direction.

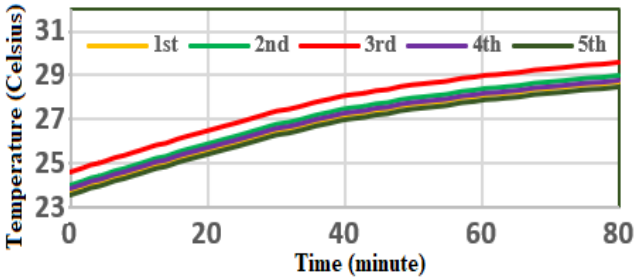

Fig. 17: experimental magnet temperature of 1st, 2nd, 3rd, 4th, and 5th sensors at 4 A 1030 rpm.

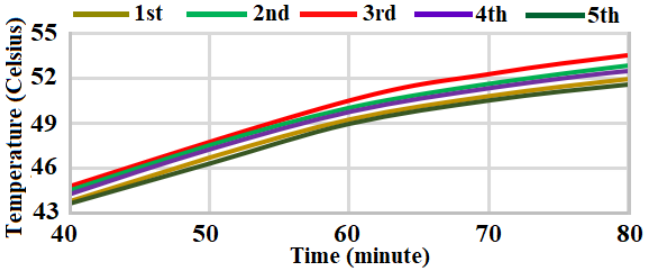

Fig. 18: experimental magnet temperature of 1st, 2nd, 3rd, 4th, and 5th sensors at 8 A 1500 rpm.

Two loading conditions: 4 A 1030 RPM and 8A 1500 RPM have been considered for experimental testing. The loading condition for experimental testing is kept limited at maximum 8A and 1500 RPM to ensure the safety of the wireless rotor setup. It should be noted that this kind of setup is not preferable for industrial use; it has been adopted to measure the magnet temperature distribution precisely for academic research purpose only.

Temperature data has been stored with a 10 minutes interval of up to 80 minutes. It has been experienced that After 80 minutes of the load operation, the magnet temperature goes to almost steady-state. Fig. 17, shows the experimental result of magnet temperature variation at 4 A 1030 RPM. It is observed that the minimum temperature of sensor-1 (blue) is 28.7^oC, and the maximum temperature is 28.7^oC in sensor 3 (red), which makes a magnet axial temperature variation of 0.62^oC. A similar phenomenon has been observed for loading condition 8A 1500 RPM as shown in fig. 18, where the magnet axial temperature variation is increased at 1.72^oC.

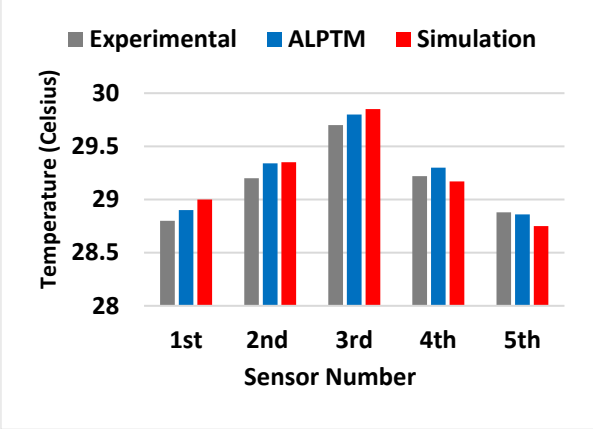

Figure 19: Comparison of thermal model, FEA, and experimental result.

The experimental result has been compared with the FEA and ALPTM, as shown in fig. 19. The difference between experimental and estimated magnet axial temperature by ALPTM is small and acceptable.

V. Conclution and Future Work

In this paper, the phenomenon of magnet axial temperature variation, and it's the impact on the electromagnetic performance of a multiphase PMaSynRM. Firstly, a novel thermal model based on the modified lumped parameter method is presented, which can estimate the temperature distribution of magnet, shaft, and coil along the axial direction, unlike conventional R-LPTM. Secondly, by using ALPTM and FEA, it is verified that the magnet axial temperature is not uniform; instead, it is nonuniform (in this case, similar to a normal curve). It is also observed that the magnet temperature increases substantially along the axial direction at higher speed and load operation. Thirdly, an algorithm has been presented to analyze the effect of magnet axial temperature variation on machine performance, especially BEMF, radial force, and torque has been studied by FEA. The results demonstrate that the increase of magnet axial temperature variation can result in uneven magnetization leading to an increase in torque ripple, machine noise, and vibration. Finally, the experimental analysis has been presented to validate the variation of the magnet temperature along the axial direction. In this case, a 5-phase PMaSynRM is used, which has a small magnet temperature gradient long axial direction due to a power rating of only 3 kW. In future work, this thermal model will be applied to the high-power density and high-speed machine.

VI. Reference

[1] A. M. Omara and M. A. Sleptsov, "Performance assessment of battery-powered electric vehicle employing PMSM powertrain system," 2017 IEEE Conference of Russian Young Researchers in Electrical and Electronic Engineering (EIConRus), St. Petersburg, 2017, pp. 963-968, doi: 10.1109/EIConRus.2017.7910716.

[2] M. Yildirim, M. Polat and H. Kurum, "A survey on comparison of electric motor types and drives used for electric vehicles", *16th Int. Power Electron. Motion Control Conf. Expo. PEMC 2014*, pp. 218-223, 2014.

[3] S. Zhang et al., "Permanent magnet technology for electric motors in automotive applications," 2012 2nd International Electric Drives Production Conference (EDPC), Nuremberg, 2012, pp. 1-11, doi: 10.1109/EDPC.2012.6425118.

[4] D. D. Reigosa, F. Briz, M. W. Degner, P. Garcia and J. M. Guerrero, "Magnet Temperature Estimation in Surface PM Machines During Six-Step Operation," in IEEE Transactions on Industry Applications, vol. 48, no. 6, pp. 2353-2361, Nov.-Dec. 2012, doi: 10.1109/TIA.2012.2227097.

[5] D. Reigosa, D. Fernandez, H. Yoshida, T. Kato and F. Briz, "Permanent magnet temperature estimation in PMSMs using pulsating high frequency current injection," 2014 IEEE Energy Conversion Congress and Exposition (ECCE), Pittsburgh, PA, 2014, pp. 5198-5205, doi: 10.1109/ECCE.2014.6954114.

[6] Gilbert, Thomas Lewis. "Formulation, Foundations and Applications of the Phenomenological Theory of Ferromagnetism." (1956).

[7] K. Liu and Z. Q. Zhu, "Online Estimation of the Rotor Flux Linkage and Voltage-Source Inverter Nonlinearity in Permanent Magnet Synchronous Machine Drives," in IEEE Transactions on Power Electronics, vol. 29, no. 1, pp. 418-427, Jan. 2014, doi: 10.1109/TPEL.2013.2252024.

[8] O. Wallscheid, T. Huber, W. Peters and J. Böcker, "Real-time capable methods to determine the magnet temperature of permanent magnet synchronous motors — A review," IECON 2014 - 40th Annual Conference of the IEEE Industrial Electronics Society, Dallas, TX, 2014, pp. 811-818, doi: 10.1109/IECON.2014.7048594.

[9] D. D. Reigosa, D. Fernandez, T. Tanimoto, T. Kato and F. Briz, "Permanent-Magnet Temperature Distribution Estimation in Permanent-Magnet Synchronous Machines Using Back Electromotive Force Harmonics," in IEEE Transactions on Industry Applications, vol. 52, no. 4, pp. 3093-3103, July-Aug. 2016, doi: 10.1109/TIA.2016.2536579.

[10] M Ganchev, C. Kral, H. Oberguggenberger, and T. Wolbank, "Sensorless rotor temperature estimation of permanent magnet synchronous motor," in *Proc. 38th Annu. Conf. IEEE Ind. Electron. Soc. (IECON)*, Nov. 2011, pp. 2018–2023.

[11] A. Arafat, M. K. Islam, J. Herbert and S. Choi, "Magnet temperature estimation based on a novel frequency determination algorithm for the five-phase PMa-SynRM," in IET Electric Power Applications, vol. 14, no. 3, pp. 357-366, 3 2020, doi: 10.1049/iet-epa.2019.0057.

[12] A. M. El-Refai, N. C. Harris, T. M. Jahns, and K. M. Rahman, "Thermal analysis of multibarrier interior PM synchronous machine using lumped parameter model," *IEEE Trans. Energy Convers.*, vol. 19, no. 2, pp. 303–309, Jun. 2004.

[13] C. Kral, A. Haumer, and S. B. Lee, "A practical thermal model for the estimation of permanent magnet and stator winding temperatures," *IEEE Trans. Power. Electron.*, vol. 29, no. 1, pp. 455–464, Jan. 2014.

[14] X. Ding, J. Liu and C. Mi, "Online temperature estimation of IPMSM permanent magnets in hybrid electric vehicles," *2011 6th IEEE Conference on Industrial Electronics and Applications*, Beijing, 2011, pp. 179-183. doi: 10.1109/ICIEA.2011.5975575

[15] L. Veg and J. Laksar, "Impact of Thermal Conductivity in Axial Direction on the Overall Thermal Model of High-Speed Synchronous Motor," 2018 XIII International Conference on Electrical Machines (ICEM), Alexandroupoli, 2018, pp. 1234-1239, doi: 10.1109/ICELMACH.2018.8506933.

[16] C. Mejuto, M. Mueller, D. Staton, S. Mebarki and N. Al-Khayat, "Thermal Modelling of TEFC Alternators," IECON 2006 - 32nd Annual Conference on IEEE Industrial Electronics, Paris, 2006, pp. 4813-4818, doi: 10.1109/IECON.2006.347908.

[17] X. Zhang et al., "The Fluid Flowing and Heat Transfer in a LSPMSM with Rotor Axial-Radial Ventilation System," 2018 21st International Conference on Electrical Machines and Systems (ICEMS), Jeju, 2018, pp. 185-190.

[18] L. Veg and J. Laksar, "Impact of Thermal Conductivity in Axial Direction on the Overall Thermal Model of High-Speed Synchronous Motor," 2018 XIII International Conference on Electrical Machines (ICEM), Alexandroupoli, 2018, pp. 1234-1239.

[19] Y. Zhang, S. McLoone and W. Cao, "Electromagnetic Loss Modeling and Demagnetization Analysis for High Speed Permanent Magnet Machine," in IEEE Transactions on Magnetics, vol. 54, no. 3, pp. 1-5, March 2018, Art no. 8200405.

[20] W. Tong, S. Wu and R. Tang, "Research on the Airflow and Thermal Performance in a Large Forced Air-Cooled Permanent Magnet Synchronous Machine," in IEEE Access, vol. 7, pp. 162343-162352, 2019.

[21] G. Du, W. Xu, J. Zhu and N. Huang, "Rotor Stress Analysis for High-Speed Permanent Magnet Machines Considering Assembly Gap and Temperature Gradient," in IEEE Transactions on Energy Conversion, vol. 34, no. 4, pp. 2276-2285, Dec. 2019.

[22] Z. Huang, J. Fang, X. Liu and B. Han, "Loss Calculation and Thermal Analysis of Rotors Supported by Active Magnetic Bearings for High-Speed Permanent-Magnet Electrical Machines," in IEEE Transactions on Industrial Electronics, vol. 63, no. 4, pp. 2027-2035, April 2016, doi: 10.1109/TIE.2015.2500188.

[23] J. Baek, S. S. R. Bonthu, S. Kwak and S. Choi, "Optimal design of five-phase permanent magnet assisted synchronous reluctance motor for low output torque ripple," *2014 IEEE Energy Conversion Congress and Exposition (ECCE)*, Pittsburgh, PA, 2014, pp. 2418-2424. doi: 10.1109/ECCE.2014.6953562